Research Journal of Applied Sciences, Engineering and Technology 3(11): 1214-1220, 2011
ISSN: 2040-7467

Submitted: July 20, 2011 Accepted: September 25, 2011 Published: November 25, 2011

The Corrosion Research on Sand Screen in the Stratum Water Saturated with CO_2

Hang Li, Yonghong Liu, Yazhou Wang, Jianmin Ma and Baoping Cai
School of Electromechanical Engineering, China University of Petroleum,
Dongying, Shandong, 257061, China

Abstract: In order to investigate the corrosion behavior of the sand screen material in stratum water, the corrosion of sand screen made of carbon/Alloy steels J55 is researched by changing the match of the Cl^-, Ca^{2+} and the HCO_3^- in the stratum water saturated with CO_2 to obtain the corrosion rate and slot width increment curve. Electron Microscopy is also used to acquire the corrosion morphology of the sample. The rule of the point corrosion and uniform corrosion is analyzed by combining the corrosion rate curve and corrosion morphology. The results show that the corrosion scale can be approximately divided into three layers. The outer layer is loose while the inner layer is compact. The corrosion rate and the slot width increment increase with the increasing of the Cl^- concentrations. However, the corrosion rate and slot width increment decrease with the increasing of the Ca^{2+} concentrations. The complexity of the HCO_3^- hydration results in the corrosion complexity. When the Cl^- concentrations are kept in a low level, serious pitting corrosion exists at most region of the sample surface. When the Cl^- concentrations rise to a high level, the surface appears uniform corrosion. The existences of the Ca^{2+} help the sample resist from the further corrosion.

Key words: Carbon/alloy steels, corrosion test, CO_2, electron microscopy

INTRODUCTION

Crude oil has become one of the most important raw materials for the production of energy and oil tube, casing and sand screen play a strategic role in oil recovery. The sand screen is particularly important as the sand production becoming more and more serious with the ongoing oil and gas field mining. The method of sand control that has been developing rapidly as sand screen has become a key factor to improve oil gas exploitation. According to the geologic features of oil and gas field at home and abroad, oil and gas field engineers put forward all kinds of new type sand control technology, such as integral cemented metal fiber screen pipe sand control technology, metal fiber sand control screen pipe sand control technology and so on. The core of the sand screen, the base pipe, does not change much. Generally speaking, the base pipe can be classified into slotted and perforated base pipe. The base pipe is not only the key of the sand screen but also is the vital part for the sand control system. Serious and uncontrollable situation occurs when the base pipe fail with all kinds of reasons. However, when the exploitation of oil and gas field came into later period, especially for extra heavy oil reservoir, sand production is severe and CO_2 is always injected into the reservoir to enhance oil recovery in engineering. Oil and stratum water mixed with CO_2 corrode sand screen especially on the base pipe rather serious during the recovery process. Serious corrosion on the base pipe may reduce the strength of the pipe and result in pipe failure. The material used to produce the base pipe is steel which is same as the material used for casing pipe. A few papers about the casing corrosion (Shayegani *et al*., 2009) can be found and used to enlighten the research on base pipe.

Carbon dioxide corrosion is commonly called sweet corrosion. This corrosion of steel is mainly a localized corrosion which appears as pits and gutters of various size and shapes. It is cause by carbon dioxide dissolving in water to form carbonic acid as water must be present to have corrosion. Lots of scholars have made great effort on this field (Zheng *et al*., 2008). Shadley *et al.* (1996) prefer to divide the corrosion process on bare metal surface into four steps. First is hydrolysis of CO_2 to form H^+, H_2CO_3 and HCO_3^-. Second step is the mass transfer of these reactant species from the bulk of the solution to the metal surface. The next step is the electrochemical reactions. The catholic reaction includes the reduction of carbonic acid into bicarbonate ions, the reduction of bicarbonate ions into carbonate ions, and the reduction of hydrogen ions. The final step is related to the mass transport of the products (Fe^{2+} and CO_3^{2-}) from the surface of the metal to the bulk of the solution. Waard and Williams (1976) considered the initial corrosion product on carbon steel is $Fe(HCO_3)_2$ and not $FeCO_3$ due to the low concentrations of CO_3^{2-}. Yin *et al.* (2008) showed that the rate-determining step depends on pH.

Corresponding Author: Hang Li, School of Electromechanical Engineering, China University of Petroleum, Dongying, Shandong, 257061, China

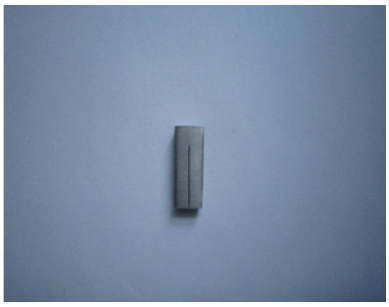

Fig. 1a: Figure of sand screen and sample

Fig. 1b: Sand screen (b) Sample

In the study of carbon dioxide corrosion, efforts have been made to investigate the influencing factor such as temperature, CO_2 partial pressure, PH and flow (Cai *et al.*, 2010). This paper aims at investigation of the effectiveness of the different ion match of the stratum water on the corrosion rate and the effectiveness of pitting corrosion on the base pipe strength.

This experiment was started to carry out at China University of Petroleum on July 4th 2010. The test material was J55 tube steel slice cut from a real sand screen by Wire Cut Electrical Discharge Machining. The sand screen and sample are shown in Fig. 1a, b. J55 chemical composition is composed of 0.34% C, 0.20% Si, 1.25% Mn, 0.02% P, 0.015% S, 0.15% Cr, 0.2Ni, 0.2% Cu and the balance of Fe. The size of each sample is measured by vernier calipers. Before the corrosion test, the surface of the sample was mechanically polished by sand paper progressively from 800 up to 2000 grades; then degreased with acetone, rinsed with 95% ethanol, weighted using a precision of 0.1 mg, and then put in the equipment as shown in Fig. 2. Before the tests began, pure N_2 was poured forcedly into the equipment and bubbled for 7h, and then the CO_2 gas was put though into the equipment for 3h; the temperature was controlled to be 90ºC and the pressure was maintained at 0.3 MPa. The corrosion test was carried out for 5d. The composition of the stratum water for each test was shown in Table 1 to 3.

Table 1: Solution composition for experiment one

Ca^{2+} (g/L)	2	2	2	2	2	2
Cl^- (g/L)	25	35	55	65	75	85
HCO_3^- (g/L)	0.2	0.2	0.2	0.2	0.2	0.2

Table 2: Solution composition for experiment two

Ca^{2+} (g/L)	2	3	4	5	6	7
Cl^- (g/L)	15	15	15	15	15	15
HCO_3^- (g/L)	0.2	0.2	0.2	0.2	0.2	0.2

Table 3: Solution composition for experiment three

Ca^{2+} (g/L)	2	2	2	2	2	2
Cl^- (g/L)	15	15	15	15	15	15
HCO_3^- (g/L)	0.2	0.3	0.4	0.5	0.6	0.7

After the corrosion test, the corrosion scale is removed by the solution (1.19 g/L HCl, 20 g/L Sb_2O_3, 50 g/L $SnCl_2$) after SEM test of the scale was finished. Then, the sample is rinsed with water and absolute ethanol, dried in natural state, and weighed again with a precision of 0.1mg for further research. Metallographical microscope and stereoscopic microscope are used to analyze cross section of the sample and sample surface morphology without corrosion scale. The magnification times are ×40 and ×20, respectively. The average corrosion rate can be described as follows:

$$V = \frac{(W_0 - W_1)}{A.t} \quad (1)$$

where, W_0 means the original weight of the sample, g; W_1 means the weight of the sample after the corrosion, g; A represents the sample surface area, m_2; t denotes the corrosion time, h.

RESULTS AND DISCUSSION

Microsturture of corrosion scale: Figure 3a shows the surface of the corrosion scale formed on J55 sample at 90ºC and 0.3 MPa for 5d. The solution composition for the sample tested by SEM is 2 g/L Ca^{2+}, 55 g/L Cl^-, 0.2 g/L HCO_3^- (Table 1-3). Part of the scale falls off from the surface of the sample as shown in Fig. 2. We name A for the upper region of the sample where the scale is kept and B for the lower part where the scale partly falls off. A represents the outer layer while B represents the inner layer. We can see clear difference between A and B from Fig. 3b. Figure 3a shows A and B respectively under higher magnification times. Figure 4a shows A which exhibits a loose and porous microstructure in corrosion scale. The crystal grains are incompact and interstitial in stacking. It seems that the outer surface of the scale tends to be falling due to the loose and porous microstructure. The Fig. 4b shows B exhibits a total different microstructure. The crystal grains are like maple leaves which are connected with each other to form a closely compact structure. This dense layer tends to prevent the

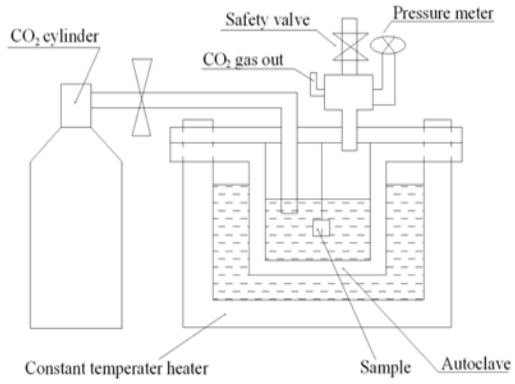

Fig. 2: Structure of experimental equipment

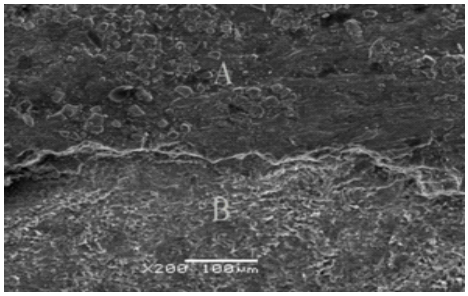

Fig. 3a: Surface morphology of scale formed on the sample magnification of 200 times

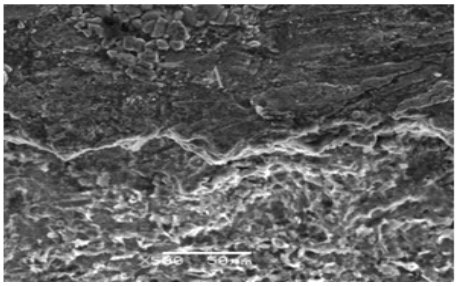

Fig. 3b: Surface morphology of scale formed on the sample magnification of 500 times

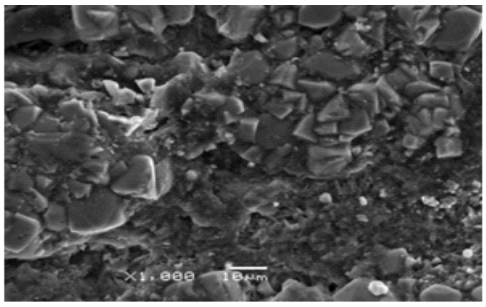

Fig. 4a: Surface morphology of region A

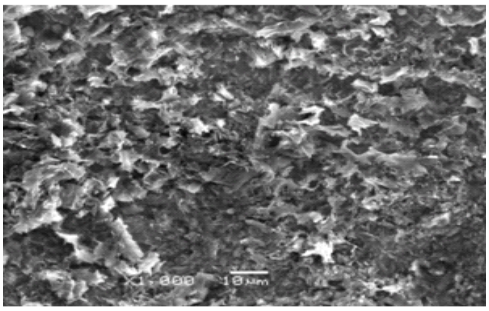

Fig. 4b: Surface morphology of region B

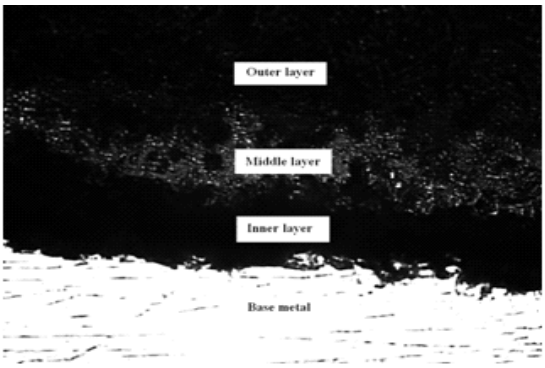

Fig. 5: Cross section of the sample

inner metal from further corrosion. Fig. 5 shows the cross-section of the scale (http://www.cibo.cn/?dictkeyword =metallographical+microscope"metallographical microscope). We can see the outer and inner layer of the scale and a middle layer exits between them. The gray middle layer is thin and permeates the outer layer and inner layer so seriously that it is difficult to clearly distinguish it with the outer and inner layer. It is slightly different from the Ref 11 about the description of the scale as the application of different pressure and temperature system.

According to the Ref 12, the combination of $FeCO_3$ and $Fe(HCO_3)_2$ (Ca^{2+} may replace Fe^{2+}) are formed initially on the sample surface and simultaneously other iron carbonate forms when Fe^{2+} and CO_3^{2-} exceed the solubility of the iron carbonate. $FeCO_3$, $Fe(HCO_3)_2$ and other iron carbonate are considered to be formed first as the outer layer. When the anions diffuse through the outer loose layer to reach the interface of the scale and substrate, $FeCO_3$ is generated and lead to the formation of the inner layer. However, some investigators (Moiseeva, 2005) hold the opinion that the inner layer is initially formed on the sample surface with porous character, and then iron ions can diffuse through the inner layer to form the outer layer. We are of the opinion that the outer layer is formed first as similar experiment condition comparing with Ref 12.

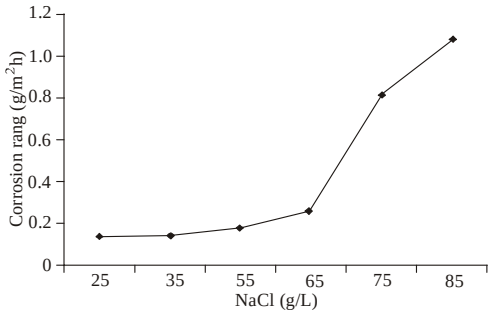

Fig. 6: Variation of corrosion rate with Cl^-

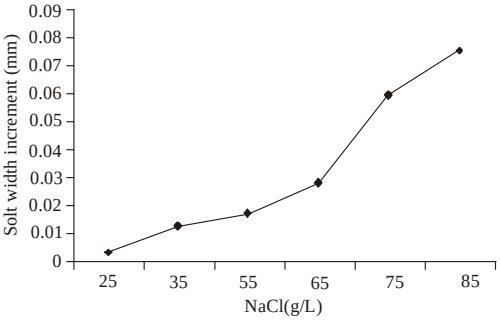

Fig. 7: Variation of slot width increment with Cl^-

The effect of Cl- on corrosion: In the following study, the scale has been removed. As we can see from Fig. 6 and Fig. 7, the corrosion rate and the slot width increment increase with the increasing of Cl^- concentrations. The corrosion rate goes up sharply when Cl^- concentrations are higher than 65 g/L; tiny changes of the corrosion rate occur with Cl^- concentrations ranging from 25 to 65 g/L. Similar trend can be found in Fig. 7. The maximum slot width increment is 0.09 mm when Cl^- concentrations are 85 g/L. The increment is so small that the effects of the slot width increment on the sand control process can be ignored. The dissolution of anode (Fe) at the effect of the Cl^- can be described as follows:

$$Fe + Cl^- + H_2O \rightarrow [FeCl(OH)]^-_{ad} + H^+ + e \quad (2)$$

$$\left[FeCl(OH)\right]^-_{ad} \rightarrow FeClOH + e \quad (3)$$

$$FeClOH + H^+ \rightarrow Fe^{2+} + Cl^- + H_2O \quad (4)$$

Such trend is in accordance with (Chen *et al*., 2003). As the Cl^- concentrations rise, the active area of the sample surface increases, leading to a higher metal dissolution rate. The existence of the Cl^- ion destroys the film formed on the surface of the sample in some degree. The uneven distribution of Cl^- ion on the sample surface makes pitting corrosion serious which can be seen from Fig. 10. Without the protection of film consisting of the iron carbonate, the pace of the corrosion rate will be accelerated. Figure 8 shows the sample surface corroded by different Cl^- concentrations. We can see from Fig. 8 that when Cl^-concentrations are low, serious pitting corrosion exists at most region of the surface. When the Cl^- concentrations reach 55 g/L, it can be found that the pitting corrosion relieves but the corrosion area extends. The pitting corrosion pits become shallower when the Cl^- concentrations are 85 g/L comparing with other lower Cl^- concentrations.

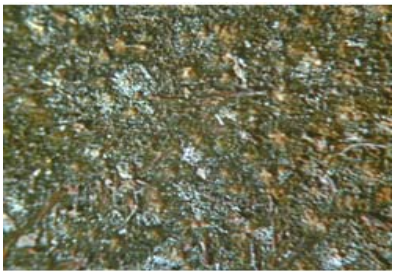

Fig. 8: Sample surface morphology varying with Cl^- without corrosion scale 85 g/L

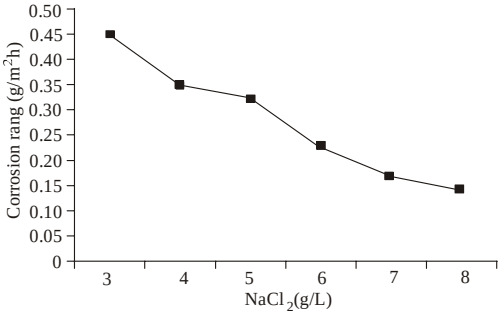

Fig. 9: Variation of corrosion rate with Ca^{2+}

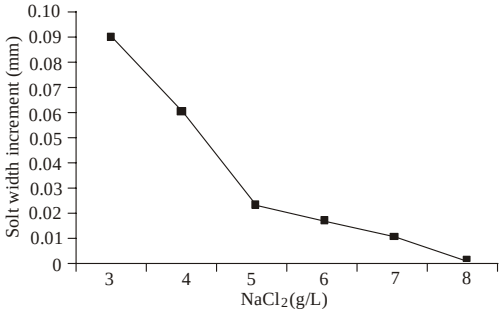

Fig. 10: Variation of slot width increment with Ca^{2+}

The effect of Ca^{2+} on corrosion: Figure 9 and 10 present the corrosion rate and slot width increment varies with the Ca^{2+} concentrations. We can see that the corrosion rate and slot width increment decrease with the increasing of the Ca^{2+} concentrations. It should be noted that

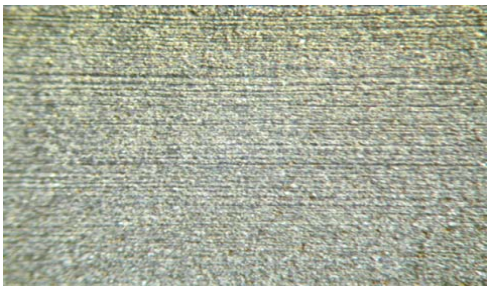

Fig. 11: Smple surface morphology varying with C^{2+} without corrosion scale 7 g/L

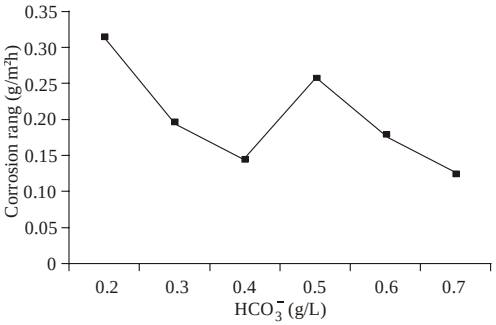

Fig. 12: Variation of corrosion rate with HCO_3^-

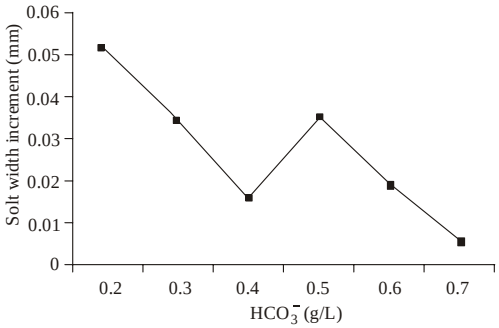

Fig. 13: Variation of slot width increment with HCO_3^-

Cl^-concentrations increase with the Ca^{2+} concentrations increasing. However, Cl^- concentrationsvary from 6 to 16 g/L and the effects of the Cl^- can be ignored within that range according to Fig. 6 and 7. The slot increment almost reaches 0 when the Ca^{2+} reaches 8g/L. This may be due to the protection of the calcium carbonate.

Figure 11 shows the sample surface corroded by different amounts of Ca^{2+} concentrations. When Ca^{2+} concentrations are 4 g/L, obvious pitting corrosion can be found on the surface. When Ca^{2+} concentrations reach to 8 g/L, pitting corrosion can hardly be found and the appearance of uniform corrosion is presented. Figure 9 and 10 clearly show that the existence of the Ca^{2+} suppresses the corrosion largely. In the solution

Fig. 14: Sample surface morphology varying with HCO_3^- without corrosion scale 0.5 g/L

containing CO_2, Ca^{2+} and CO_3^- combine together coating on the surface with iron carbonate to avoid further corrosion to the sample to some extent. When the Ca^{2+} concentrations are low, $CaCO_3$ and iron carbonate do not cover the sample surface thoroughly and some region expose to the solution. There may be a galvanic corrosion with strong catalytic properties between different coverage regions and this may accelerate the corrosion rate of exposed area. When Ca^{2+} concentrations reach a high level, most area of the surface is covered by the combination of $CaCO_3$ and iron carbonate. The active area of the sample surface reduces and the corrosion rate decreases. The point mentioned in (Jiang *et al.*, 2006) that the corrosion rate increases with the Ca^{2+} concentrations increasing is totally different from the point mentioned above. This is probably due to the application of different solution PH and pressure condition.

The effect of HCO_3^- on corrosion: We can see from Fig. 12 and 13 that the HCO_3^- affects the corrosion process in a complex way. The balance equation of CO_2, HCO_3^- and CO_3^{2-} is as follows:

$$CO_2+H_2O \Leftrightarrow HCO_3^-+H^+ \quad (5)$$

$$HCO_3^- \Leftrightarrow CO_3^{2-}= H^+ \quad (6)$$

Equation (1) moves to the left inducing the CO_2 overflow from the solution with the increasing of the HCO_3^- concentrations. This trend decreases the H^+ concentrations. It is reasonable to accept the fact that the corrosion rate is decreasing. However, according to Eq. (2), the increasing of HCO_3^- promotes the Eq. (2) moving to the right, which boosts the increasing of H^+. Such trends prefer to increase the corrosion rate. The complexity of the HCO_3^- hydrolysis in the solution leads to the complex corrosion process. Moreover, Mg^{2+}, Ca^{2+} and Ba^{2+} in the stratum which are prone to be combined with the CO_3^{2-} to make the HCO_3^- hydrolysis more complicated. The corrosion process becomes so hard to be predicted because of the complex HCO_3^- hydrolysis.

Figure 14 shows the sample surface corroded by different HCO_3^- concentrations. We can see that Fig. 14 presents the appearance of uniform corrosion. The corrosion degree varies with different HCO_3^- concentrations. It seems that the sample is more prone to be corroded in the solution with lower HCO_3^- concentrations. This can be seen from Fig. 12.

CONCLUSION

According to the SEM profiles, the corrosion scale can be roughly divided into outer layer, middle layer and inner layer. The middle layer between them is thin and difficult to be peeled apart from outer or inner layer. The corrosion rate and the slot width increment increase with the increasing of Cl^- concentrations but decrease with the increasing of the Ca^{2+} concentrations. The effect of HCO_3^- for sample corrosion is complicated due to the complexity of the HCO_3^- hydrolysis. Serious pitting corrosion exists at most region of the surface when Cl^- concentrations are low. The corrosion region extends when the Cl^- concentrations reach a high level. The existence of Ca^{2+} provides protection to the steel basic phase.

ACKNOWLEDGMENT

This research is sponsored by National High-Technology Research and Development Program of China ("863"Program) (NO. 2007AA09A101) and National Natural Science Foundation of China (NO. 50874115).

REFERENCES

Cai, Y., G. Pengchao, D. Liu, S. Chen and J. Liu, 2010. Comparative study on CO_2 corrosion behavior of N80, P110, X52 and 13Cr pipe lines in simulated stratum water. China. Technol., 53(9): 2342-2349.

Chen, C., M. Lu, G. Zhao and Z. Bai, 2003. Effects of temperature, Cl^- concentration and Cr on electrode reactions of CO_2 corrosion of N80 steel. Act. Metall. Sin., 39(8): 848-853.

Jiang, X., Y.G. Zheng, D.R. Qu and W. Ke, 2006. Effect of calcium ions on pitting corrosion and inhibition performance in CO_2 corrosion of N80 steel. Corros, 48(10): 3091-3108.

Moiseeva, L.S., 2005. Carbon dioxide corrosion of oil and gas field equipment. Prot. Met., 41(1).

Shadley, J.R., S.A. Shirazi, E. Dayalan, M. Ismail and E.F. Rybicki, 1996. Erosion-corrosion of a carbon steel elbow in a carbon dioxide environment. Corrosion, 52(9): 714-723.

Shayegani, M., M. Ghorbani and A. Afshar, 2009. Rahmaniyan. Modeling of carbon dioxide corrosion of steel with iron carbonate precipitation. Corros. Eng. Technol., 44(2): 128-136.

Waard, C.D. and D.E. Williams, 1976. Prediction of carbonic acid corrosion in natural gas pipelines. Ind. Finish Surface Coat., 28(340): 24-28.

Yin, Z., W. Zhao, Z. Bai and Y. Feng, 2008. Characteristic of CO2 corrosion scale formed on P110 steel in stimulant solution with saturated CO_2. Surf Interface Anal, 40(9): 1231-1236.

Zheng D., D. Che and Y. Liu, 2008. Experimental investigation on gas-liquid two-phase slug flow enhanced carbon dioxide corrosion in vertical upward pipeline. Corros., 50(11): 3005-3020